

# Mesh-based Computation for Solving Photometric Stereo with Near Point Lighting

Wuyuan Xie, Ying Nie, Zhan Song and Charlie C.L. Wang, *Senior Member*

**Abstract**— We tackle the problem of dense reconstruction with a practical system, in which near point lighting is employed. Different from the conventional formulation of photometric stereo that assumes parallel lighting, photometric stereo under the *near point lighting* (NPL) condition is a nonlinear problem as the local surface normals are coupled with its distance to the camera as well as the light sources. After obtaining the locations of point lights by a calibration process, we develop a new framework to solve this nonlinear reconstruction problem via mesh deformation, in which each facet is corresponding to a pixel in the image captured by the camera. In our framework, mesh deformation is decoupled into an iteration of interlaced steps of local projection and global blending. Experimental results verify that our method can generate accurate estimation of surface shape under NPL in a few iterations. Besides, this approach is robust to errors on the positions of light sources and is easy to be implemented.

**Index Terms**— 3D reconstruction, photometric stereo, near point lighting, practical system.

## I. INTRODUCTION

The reconstruction of 3D geometry is very important in many robotics and automation applications. Reconstructing 3D geometry as a feedback can help improve performance of mechatronics systems in different applications – e.g., 3D printing, grasping, surgery and machining. Comparing to the existing techniques such as reconstruction by motion, time-of-fly, infrared etc., the technique using *photometric stereo* (PS) is considered as an easy to be implemented method with low-cost hardware. Specifically, PS [1] estimates a dense field of normals from a set of 2D images captured by a fix camera under different illumination conditions. In the framework of PS, it is assumed that objects to be reconstructed all have a Lambertian surface and are illuminated by at least three known lighting directions. As a result, the normal vector at each pixel can be determined from the captured image intensities uniquely (or by a least-square solution when more than three images are taken). Such a simple principle makes PS as an old but distinctive topic in computer vision developed for decades.

### A. Motivation

Traditional *photometric stereo* (PS) has advantage on capturing the geometry details in high frequency but has defects in reconstructing good overall shapes in low frequency.

Revised manuscript submitted in July 2016.

W. Xie is with Chinese University of Hong Kong. Y. Nie and Z. Song are with Shenzhen Institutes of Advanced Technology, Chinese Academy of Sciences. C.C.L. Wang is with Delft University of Technology, The Netherlands.

Corresponding Author: Charlie C.L. Wang (Tel: +31 (0)15 27 88406; E-mail: c.c.wang@tudelft.nl).

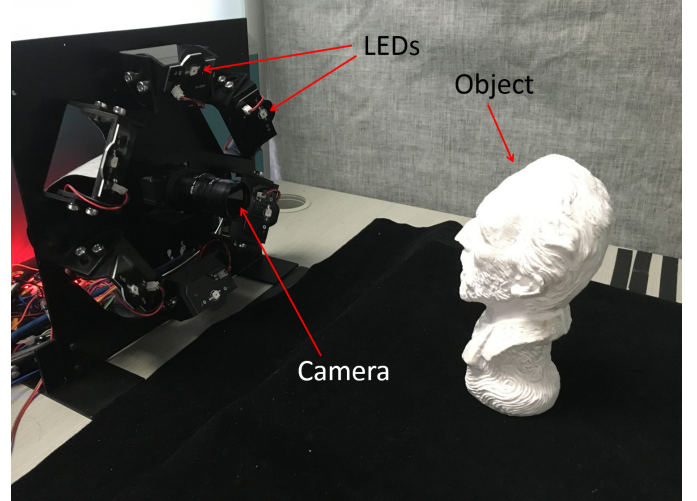


Fig. 1. In our system, six infrared LEDs (OSRAM SFH4232A) are placed around a calibrated camera (Point Gray FLFL3-U3-13S2C-CS) with short distance to an object to be reconstructed.

The shape distortion is caused by many factors such as the accumulation of reconstruction errors during the integration, etc. In this work, we tackle the distortion sourced from the assumption of parallel lighting, which enable the problem to be linearized into a set of linear equations to be solved by the least-square solution in conventional PS. To achieve the parallel lighting, light sources should be placed far away from the object, which however would make its luminance attenuate sharply to result in the captured images of poor quality. Hence, in practical hardware prototypes, light sources are usually placed with short distance to the object as shown in Fig.1 to guarantee the light intensity on pixels. Correspondingly, PS problem becomes nonlinear – also called *near point lighting PS* (NPL-PS), where the lighting directions become nonuniform (see Fig.1) that should be coupled with depth in the computation of surface normals. In this paper, we provide a mesh-based solution to the problem of *near point lighting PS* (NPL-PS) without using integrability constraints or auxiliary sparse map. Noted that, our method does not limit the surface to have  $C^2$  or  $C^1$ -continuity, which is common requirement in others PS works. Instead, we are able to reconstruct surfaces with  $C^0$ -continuity. For models with discontinuity, the regions of cracks must be explicitly specified on the input images to generate cracks on the mesh models as well.

Without loss of the generality, the input of our NPL-PS approach has  $k$  images,  $\mathcal{I}_1, \dots, \mathcal{I}_k$ , where each has the same interested region composing of  $m$  pixels. The image  $\mathcal{I}_i$  is

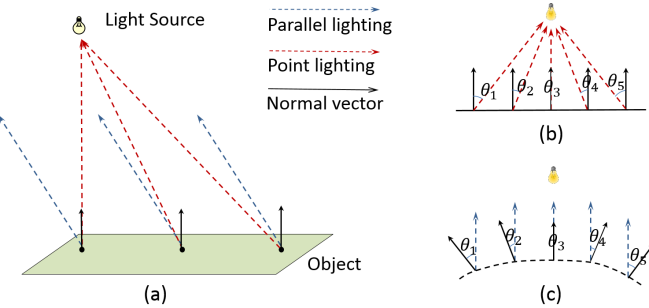


Fig. 2. NPL-PS with parallel lighting assumption on a plane (a) will lead to spherical distortion as illustrated in the change from (b) to (c).

captured under the illumination of the  $i$ -th lighting source with its position  $\mathbf{p}_i \in \mathbb{R}^3$  known. As illustrated in Fig.2 (a), different surface points have different lighting directions under the illumination of near point lighting. The lighting direction at a point corresponding to a pixel in the image space not only varies with the change of image coordinates but also changes according to the depth. In short, the radiation model correlating the captured light intensities and the height/orientation of a surface region is nonlinear.

### B. Related work

Prior works have paid a lot of attention to improve the results of PS-based reconstruction – mainly by correcting the aforementioned assumptions for linearization. For the PS system utilized near point light sources, the non-uniform lighting can greatly decrease the 3D reconstruction quality. To solve this problem, a model based on *partial differential equations* (PDE) was introduced to approximate the near-field lighting in [2], and a lighting compensation-based approach was presented in [3] to make the image intensity more homogeneous. The emitting characteristics of light sources were considered in the PS algorithm to improve the modeling accuracy of the light sources [4]. However, to describe the near point lighting precisely is a complicate issue which should consider the factors including light source characteristics, objective distance, surface shape and reflectance. In comparison, 3D reconstruction quality by existing NPL-PS methods is usually worse than the PS systems that adopt parallel or distant point light sources.

Supposing the surface to be reconstructed is under ideal diffuse-reflection, the surface normals estimated by PS are mainly affected by the lighting directions. In most PS hardware prototypes, light sources cannot be assumed as parallel lighting. Considering this, PS problem becomes nonlinear and the numerical computation based on nonlinear optimization requires other auxiliaries or assumptions (e.g., with some known 3D positions or integrability assumptions). According to the strategy of eliminating the lighting direction uncertainty caused by near lighting condition, existing NPL-PS methods can be classified into two major categories: 1) PS based on integrability assumption and 2) PS required auxiliary means.

- 1) Methods in this category solve the light direction ambiguity problem based on the assumption that the shape

is continuous and smooth (e.g., [5]–[9]). Absolute depth is directly estimated under the framework of NPL-PS with perspective projection in [5]. This method requires the surface to be integrable and having uniform albedo. The ambiguity of light direction in NPL-PS is solved in [6] by strictly controlling the motion of light sources. Besides, for some special PS hardware prototypes, dedicated NPL-PS methods have been introduced. In [7], a NPL-PS method is proposed for a PS hardware with 20 light sources uniformly distributed on a ring. They compare and analyze the affects from six common assumptions which are usually taken in parallel PS, and incorporate these factors into the optimization. To obtain a good result of reconstruction, hundreds of images are required. A model with rectangular light sources (by using LCD monitor) is formulated in [8] for NPL-PS. All the above methods require the surface to be integrable such that the unknown lighting direction can be represented by depth for optimization. The results always have shape distortion in a certain level as the requirement of integrability cannot be strictly satisfied – especially on the real objects. Recently, a new NPL-PS method is proposed in [9] for a compact PS hardware prototype with light sources in small angular variations. They involve quite a few possible factors that might affect the normal calculation into the objective function, and prove that such an objective function can converge to an acceptable results if a good initialization is given. Our approach attempts to solve the problem by the means of using a novel mesh deformation approach.

- 2) For the auxiliary means based PS, the shape of results can be preserved better by giving some geometry constraints such as known depths on a few points (e.g., [10], [11]). NPL-PS is performed in a contact way in [10] to locally scanning the geometric details on a surface. Their work can reconstruct the micro-geometry of a surface but fails to give the correct global shape. Different, A sparse depth-map or scattered 3D feature points are used in [11]. Instead of knowing a sparse map as auxiliary quantity to guide the shape estimation, we only need to know the shift between the image coordinate system and the world coordinate system, which is used for the initialization of depth.

Recently, effort has been made to further enrich the techniques for NPL-PS. Liao et al. [12] propose an uncalibrated computational system for NPL-PS, where variance of lighting is captured by moving the light sources away from the scene. Their method allows less than three input images; however, they require the rail of light sources be strictly aligned on a straight line. Differently, we conduct a mesh-based deformation method to provide a discrete solution for the nonlinear NPL-PS problem, where our computation converges very fast. This paper is an extended version of [13] with implementation on a practical lighting system, where our prior work is mainly based on images captured in virtual lighting environments. The calibration method for determining the positions of light sources has been developed. More experimental tests and

discussion have been taken on the hardware prototypes to verify the performance of our system.

In the literature of geometric modeling, the local/global optimization strategy has been widely used to decouple the problem of solving nonlinear optimization into interlaced orthogonal linear operations (e.g., [14]). Recently, the discrete geometric processing technique has been extended to solve the surface-from-gradients problem [15]. Inspired by this work, we develop a new method to solve the NLP-PS problem by mesh deformation. Unlike the conventional pipeline of PS that computes a dense normal field first and then conducts the surface-from-gradients technique to obtain the surface shape, we provide a one-stop solution to directly generate a 3D surface from the input 2D images. Details can be found in Section IV.

### C. Contribution

The technical contributions of our work presented in this paper are mainly in the following aspects:

- In this paper, we propose a NPL-PS method to reconstruct a continuous surface without assuming it to be integrable. It give the possibility to the PS dedicated to reconstruct the surface with  $C^0$ -continuity.
- Shape distortion is a common weakness among NPL-PS and PS methods. The proposed NPL-PS method does not rely on any auxiliary means but can still guarantee the global shape of results.
- The nonlinear NPL-PS problem is solved by a mesh deformation approach with iteratively applied local shaping and global blending steps. Only simple linear operations are taken in our approach during the iterations.

As a result, a 3D mesh surface can be efficiently and robustly reconstructed from shaded images captured by our system, and the computation of reconstruction can be completed after only a few steps of mesh deformation. Both the geometric details in high frequency and the overall shapes in low frequency can be accurately reconstructed on the resultant mesh surface.

The rest of this paper is organized as follows. We analyze and compare the difference between conventional PS and NPL-PS in Section II. After that, a calibration method is introduced in Section III to determine the positions of point light sources. The formulation for solving the NPL-PS problem is detailed in Section IV. Lastly, experimental results are given in Section V, and our paper ends with the conclusion section.

## II. LINEAR VS. NONLINEAR PHOTOMETRIC STEREO

In this section, we analyze the problem of conventional PS framework (i.e., linear PS) and then introduce the NPL-PS model that is nonlinear.

### A. Conventional photometric stereo

The observed appearance brightness  $I$  of a Lambertian object under a lighting direction  $\mathbf{l} \in \mathbb{R}^3$  at a surface point  $\mathbf{x} \in \mathbb{R}^3$  can be described as  $I(\mathbf{x}) = \rho \mathbf{n} \cdot \mathbf{l}$ , where  $\rho$  is the nonuniform Lambertian reflection albedo and  $\mathbf{n} \in \mathbb{R}^3$  is

the surface normal at  $\mathbf{x}$ . Note that, under the assumption of parallel lighting in conventional PS, the lighting direction does not change in the whole domain (i.e.,  $\mathbf{l}$  is *not* a function of  $\mathbf{x}$ ). There are  $k$  images,  $\{\mathcal{I}_i\}$ , of the same object under the illumination of different light sources, and the above lighting model is used to determine the value of  $\mathbf{n}$  at each pixel in the interested region. Specifically, when  $k > 3$ , the value of  $\rho \mathbf{n}$  can be determined by a least-square solution of

$$I_i(\mathbf{x}) = \rho \mathbf{n} \cdot \mathbf{l}_i \quad (i = 1, \dots, k). \quad (1)$$

Here,  $I_i$  is the brightness observed in the  $i$ -th image and  $\mathbf{l}_i$  denotes the lighting direction of the  $i$ -th source. Different values of the Lambertian reflection albedo appear at different surface points. However, the value of  $\rho$  does not change at the same surface point under the illumination of different lighting directions. As a result, one can solve Eq.(1) to obtain the value of  $\rho \mathbf{n}$  first, and then normalize it to obtain a unit surface normal vector  $\mathbf{n}$ . After that, the surface-from-gradients technique (e.g., [15]) is employed to reconstruct a 3D surface from the field of normal vectors.

### B. Near point lighting illumination

The conventional PS assumes an object to be reconstructed is under the illumination of nearly parallel lighting. In practice, illumination is nearly parallel only when the distance between a lighting source and the object is more than 10 times of the object's dimension. However, when a light source is placed in a distance that far away from the object, the luminance will attenuate sharply so that normal evaluation based on light intensity will have large error. Based on this reason, light sources are usually placed close to the object to ensure the quality of images. In such circumstances, parallel lighting assumption leads to the significant shape distortion in coarse scale although the geometric details in high-frequency band can still be successfully reconstructed.

To overcome this contradiction between assumption and practice, we adopt the near point lighting (NPL) model to estimate the surface shape in this paper. Under the illumination of NPL, two important factors must be noticed.

- Every surface point has its own unique lighting direction, and all lighting directions at different regions converge at the same point light source.
- The attenuation of luminance needs to be considered in the Lambertian radiance model (i.e., distances between surface points and light sources should be incorporated into the model).

Therefore, akin to the lighting model presented in [16], we employ a NPL model as

$$I_i(\mathbf{x}) = \frac{\rho}{\alpha \|\mathbf{p}_i - \mathbf{x}\|^2} \left( \mathbf{n}(\mathbf{x}) \cdot \frac{\mathbf{p}_i - \mathbf{x}}{\|\mathbf{p}_i - \mathbf{x}\|} \right), \quad (2)$$

where  $\alpha$  is the attenuation coefficient,  $\mathbf{p}_i$  is the position of the  $i$ -th light source, and therefore  $(\mathbf{p}_i - \mathbf{x})/\|\mathbf{p}_i - \mathbf{x}\|$  gives the lighting direction  $\mathbf{l}_i$  at  $\mathbf{x}$ . The difference between this illumination model and the conventional illumination model in PS has been explained and illustrated in Section I-A.

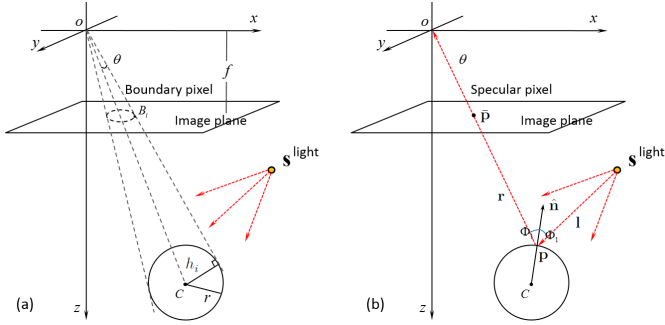


Fig. 3. An illustration for the principle of calibration: (a) for the center of a sphere and (b) for the light direction by reflection model of  $\hat{\mathbf{n}}$ ,  $\mathbf{r}$  and  $\mathbf{l}$ .

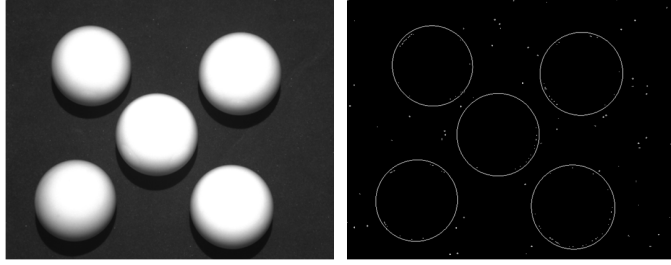


Fig. 4. Using a photo under bright illumination (left), boundary points can be selected from the result of edge extraction (right).

In our NPL model, the position of light sources can be obtained by a calibration procedure (see Section III) when the relative position between camera and light sources are fixed during the shape acquisition. Even after determining the positions of light sources, Eq.(2) is still non-linear due to the unknown depth value of  $x$  for each pixel in the captured images. In the following, we investigate a method to solve the values of  $\mathbf{n}(x)$  and  $x$  simultaneously based on local/global mesh deformation. Besides the positions of light sources, our method also needs to know the corresponding width  $w$  and height  $h$  of a pixel in the captured images – i.e., scale of the image coordinates to the Euclidean coordinates, which can also be obtained from the calibration procedure.

### III. CALIBRATION

In this section, the method to calibrate the positions of light sources in our system is presented. The calibration method is akin to our prior work for parallel lighting; however, more but not one shiny semi-spheres are employed here for determining the positions of light sources (i.e.,  $\mathbf{p}_i \in \mathbb{R}^3$ ). After calibrating the camera for its focal length  $f$  and principle point  $O$  by [17], our calibration is taken in two steps following the process of [18]. First, the centers of spheres are determined. Second, the positions of light sources are computed by using the images of illuminated spheres.

#### A. Centers of spheres

Selecting the coordinate system of the camera as the coordinate for illustration, the center of a sphere can be determined according to the following two observations:

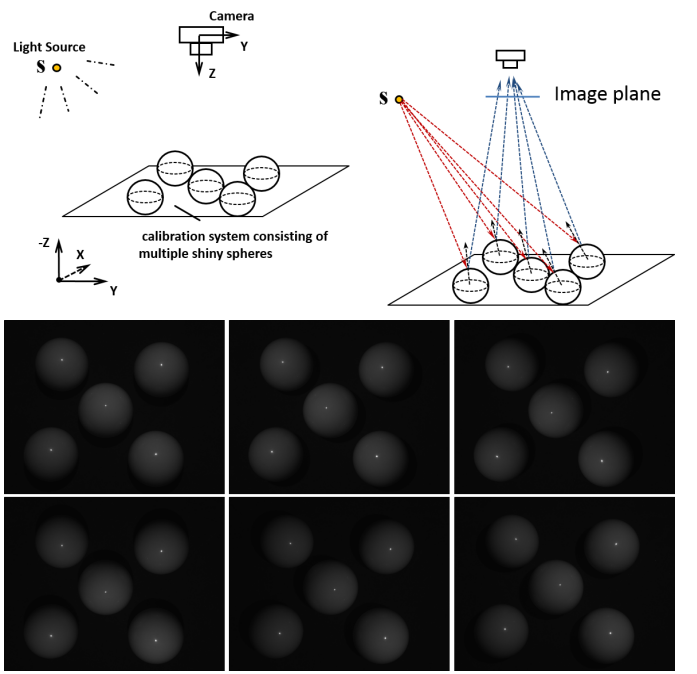


Fig. 5. Calibration with multiple spheres. (Top) An illustration. (Bottom) Photos captured in the calibration using five shiny spheres under the illumination with six different point light sources, where each photo is used to determine the position of one point light source.

- any line passing through the camera center and a boundary point of the sphere in the image plane is tangential to the sphere;
- the distance from the center of a sphere to a tangent line is the radius of the sphere.

Therefore, as illustrated in Fig.3(a), we can have

$$h_i^2 = |OC|^2(1 - \cos^2 \theta) \quad (3)$$

with

$$\cos \theta = \frac{OC \cdot OB_i}{|OC||OB_i|} = \frac{\sqrt{|OC|^2 - h_i^2}}{|OC|}, \quad (4)$$

where  $B_i$  a boundary point on the image plane with a checked position  $(x_i, y_i, f)$ , and  $h_i$  the distance between the sphere center and the tangent line  $OB_i$ . Only the center of sphere is an unknown in Eq.(3).

By capturing an photo with the spheres under bright illumination, candidates of boundary points can be obtained by the Canny edge extraction (see Fig.4). In our implementation,  $m = 7 \sim 10$  boundary points are interactively picked for each sphere. The center of each sphere can then be determined by minimizing the energy

$$E = \sum_{i=1}^m (h_i^2 - r^2)^2, \quad (5)$$

where the radius  $r$  of a sphere is measured beforehand.

#### B. Positions of light sources

For computing the position of a light source, we first consider the reflection model on one sphere and one point light source as illustrated in Fig.3(b). The point light source,

$S$ , illuminates rays with variant angles. Since the sphere has a shiny surface, there must be a specular point on its surface which would cause specular reflection. The corresponding specular pixel  $\bar{p}$  on the image plane can be captured by the camera. We detect  $\bar{p}$  by finding the brightest pixel in an image.

After that, based on the parameters of sphere obtained in the above sub-section, we can determined the corresponding 3D point  $p$  of  $\bar{p}$  on the sphere. Meanwhile, the surface normal  $\hat{n}$  at  $p$  can be obtained. Finally, we can calculate the lighting direction  $l$  to the specular point  $p$  by

$$l = 2(\mathbf{r} \cdot \hat{\mathbf{n}})\hat{\mathbf{n}} - \mathbf{r} \quad (6)$$

with  $\mathbf{r} = -\mathbf{p}$ . By this method, one shiny sphere can be used to determine one lighting ray from  $S$ . Hence, as shown in Fig.5, if more shiny spheres placed in different positions are used, we can estimate the position of  $S$  as the ‘intersection’ of lighting rays determined on these spheres. However, there are errors embedding in the calibrated parameters and the captured images, these rays rarely share any common point in practice. The position of  $S$  is then determined as a point that minimizes the total squared distance to all of these rays. To decrease the system error, we improved our calibration system by adding up to five shiny spheres. Point light source used in our setup are calibrated one by one using this method (as shown in the bottom of Fig.5).

#### IV. NPL-PS BY MESH DEFORMATION

Our formulation for solving the NPL-PS problem is based on converting each pixel  $(i, j)$  in the interested region into a quadrangular facet  $f_{i,j}$ , the boundary of which is defined by four vertices  $\mathbf{v}_{i,j}$ ,  $\mathbf{v}_{i+1,j}$ ,  $\mathbf{v}_{i+1,j+1}$  and  $\mathbf{v}_{i,j+1}$ . A vertex  $\mathbf{v}_{i,j}$  has its  $x$ - and  $y$ -coordinates fixed and  $z_{i,j}$  as an unknown variable to be determined – that is  $(o_x + iw, o_y + jh, o_z + z_{i,j})$ . Here  $(o_x, o_y, o_z)$  specifies the shifting between the image coordinate system and the world coordinate system. The initial values of  $z_{i,j}$ s can be assigned as  $z_{i,j} = 0$  or be given randomly. The following formulation will provide an efficient method to determine their values to satisfy Eq.(2) on all facets/pixels. The collection of facets forms a mesh surface  $\mathcal{M}$  with  $C^0$ -continuity. As mentioned in Section I, discontinuity must be introduced on the mesh in advance if there is some. Our algorithm introduce below will not be able to generate cracks automatically.

##### A. Local/Global mesh deformation

Generally speaking, the strategy of local/global mesh deformation decouples the nonlinear optimization procedure into interlaced steps of local shaping and global blending. A mesh surface  $\mathcal{M}$  is deformed iteratively to minimize an energy function defined according to the governing conditions (e.g., enforcing normals to follow the input gradient-field).

In each iteration, a local shaping step is first performed to determine the position and orientation of each facet according to its target normal and its current shape. The mesh surface has been broken after the local shaping – see Fig.6 for an illustration. After that, a global blending step is applied to glue all the facets back into a connected mesh surface. Specifically,

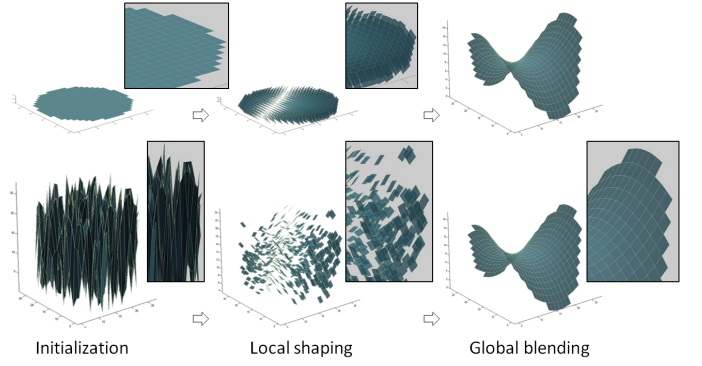


Fig. 6. One step of our mesh deformation based NPL-PS: (left) an initial mesh surface before deformation, (middle) the facets are positioned along the orientation of target normals in the local shaping step, and (right) the facets are glued together into a mesh surface in the global blending step. The final result can be obtained by applying the steps of local shaping and global blending iteratively. It is easy to find that our method is trivially affected by the initial guess. When a planar initial shape (top row) or a random initial shape (bottom row) is given, the computation converges to the similar shape in just a few steps.

the global blending step minimizes a functional to reduce the difference between  $\mathbf{z}(f_{i,j})$  and  $\mathbf{q}(f_{i,j})$  on each facet  $f_{i,j}$ , where  $\mathbf{z}(f_{i,j})$  is a column vector formed by the depths of  $f_{i,j}$ 's four vertices

$$\mathbf{z}(f_{i,j}) = \{z_{i,j}, z_{i+1,j}, z_{i+1,j+1}, z_{i,j+1}\},$$

and  $\mathbf{q}(f_{i,j})$  is its corresponding vector after applying the local shaping step. Details for determining  $\mathbf{q}(f_{i,j})$  can be found in Section IV-B. However, enforcing  $\mathbf{z}(f_{i,j}) = \mathbf{q}(f_{i,j})$  is too restrictive, which could slow down the convergence during the iteration. To solve this problem, the functional is relaxed by applying the mean-subtraction technique (ref. [14]) as

$$\Phi(\{z_{i,j}\}) = \sum_{f_{i,j}} \|\mathbf{Nz}(f_{i,j}) - \mathbf{Nq}(f_{i,j})\|^2, \quad (7)$$

where  $\mathbf{N} = \mathbf{I}_{4 \times 4} - \frac{1}{4}\mathbf{1}_{4 \times 4}$  with  $\mathbf{1}$  being a matrix with all elements equal to 1. It is found that Eq.(7) can be reformulated into a more compact form as

$$\Phi(\{z_{i,j}\}) = \|\mathbf{Ad} - \mathbf{b}\|^2, \quad (8)$$

where  $\mathbf{A}$  is a  $4m \times n$  matrix derived from  $\mathbf{Nz}(f_{i,j})$  and  $\mathbf{b}$  is a vector with  $4m$  components derived from  $\mathbf{Nq}(f_{i,j})$  on a mesh surface  $\mathcal{M}$  with  $m$  quadrangular facets and  $n$  vertices. All the unknown depth values of the vertices ( $n$  in total) are listed in  $\mathbf{d}$ . This is a standard least-square problem, which can be solved by  $\mathbf{A}^T \mathbf{Ad} = \mathbf{A}^T \mathbf{b}$ . Moreover,  $\mathbf{A}^T \mathbf{A}$  does not change during the iterations as the matrix  $\mathbf{A}$  only depends on the connectivity of  $\mathcal{M}$  that is invariant. As a result, we can pre-factorize  $\mathbf{A}^T \mathbf{A}$  at the beginning of iterations and re-use the result of factorization in all the rest steps – the computation only involving back substitution is very efficient.

##### B. Local projection for NPL-PS

To use the local/global mesh deformation technique, we first formulate the local shaping step of each facet according to the lighting model that has been derived in Section II for NLP-PS. Considering about a pixel  $(i, j)$  and its corresponding

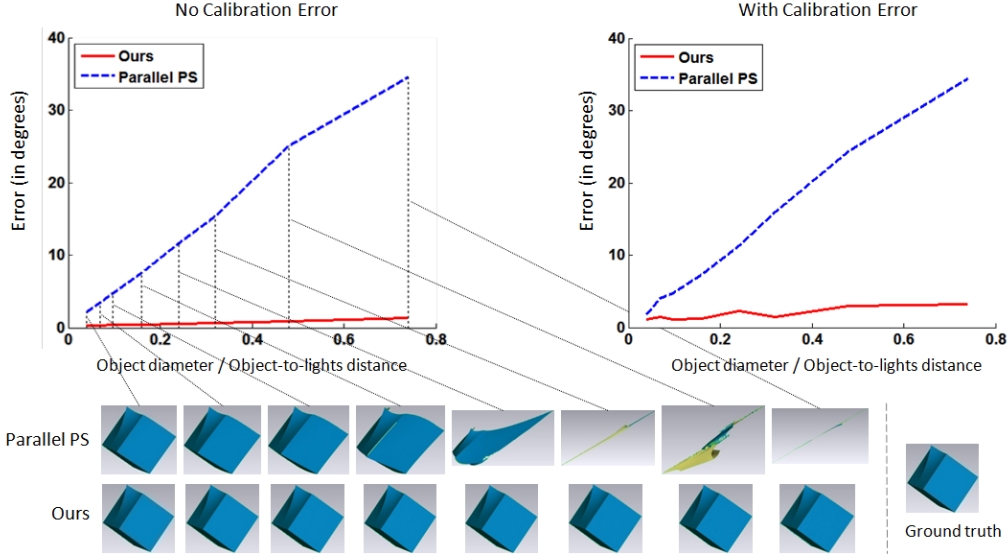


Fig. 7. Comparison in the virtual environment by using 1) images taken in the exposure of far point lighting in the parallel PS to 2) images taken in the NPL exposure in our framework. To obtain nearly parallel lighting in case 1), the light sources must be placed far ways from the object to be reconstructed. This comparison is actually as using the left point on the blue curve to compare with other points on the red curve. Here it assumes a very strong light source. In practice, when a light-source with lower intensity is employed – resulting in very dark images, larger errors will be generated on the reconstruction from parallel PS.

facet  $f_{i,j}$ , two operations are taken on  $f_{i,j}$  for solving the NPL-PS problem in the local shaping step: 1) determining the normal,  $\mathbf{n}_{i,j}$ , of  $f_{i,j}$  and 2) rotating the facet to following the orientation of  $\mathbf{n}_{i,j}$ .

The normal  $\mathbf{n}_{i,j}$  is determined at the center of  $f_{i,j}$ , that is  $\mathbf{c}_{i,j} = \frac{1}{4}(\mathbf{v}_{i,j} + \mathbf{v}_{i+1,j} + \mathbf{v}_{i+1,j+1} + \mathbf{v}_{i,j+1})$ . Thus, for the  $k$ -th image, an equation can be obtained from the nonlinear lighting model at  $\mathbf{c}_{i,j}$  from Eq.(2) as

$$(\mathbf{p}_k - \mathbf{c}_{i,j}) \cdot \frac{\rho}{\alpha} \mathbf{n}_{i,j} = I_k(i,j) \|\mathbf{p}_k - \mathbf{c}_{i,j}\|^3, \quad (9)$$

where  $I_k(i,j)$  denotes the light intensity at the pixel  $(i,j)$  in the image  $\mathcal{I}_k$ . Incorporating all images, we can have  $m$  such constraints in Eq.(9) with  $k = 1, \dots, m$ . This gives an over-determined linear system with dimension  $m \times 3$ . The normal vector  $\mathbf{n}_{i,j}$  can be obtained by a least-square solution multiplying both sides with transpose of the  $m \times 3$  coefficient matrix, which results in a normal equation as

$$\mathbf{T} \left( \frac{\rho}{\alpha} \mathbf{n}_{i,j} \right) = \sum_k \|\mathbf{p}_k - \mathbf{c}_{i,j}\|^3 I_k(i,j) (\mathbf{p}_k - \mathbf{c}_{i,j}) \quad (10)$$

with

$$\mathbf{T} = \begin{bmatrix} \sum_k (\mathbf{a}_k^x)^2 & \sum_k (\mathbf{a}_k^x \mathbf{a}_k^y) & \sum_k (\mathbf{a}_k^x \mathbf{a}_k^z) \\ \sum_k (\mathbf{a}_k^x \mathbf{a}_k^y) & \sum_k (\mathbf{a}_k^y)^2 & \sum_k (\mathbf{a}_k^y \mathbf{a}_k^z) \\ \sum_k (\mathbf{a}_k^x \mathbf{a}_k^z) & \sum_k (\mathbf{a}_k^y \mathbf{a}_k^z) & \sum_k (\mathbf{a}_k^z)^2 \end{bmatrix} \quad (11)$$

by defining  $\mathbf{a}_k = \mathbf{p}_k - \mathbf{c}_{i,j}$ . The superscript in  $\{x, y, z\}$  indicates the  $x$ -,  $y$ - and  $z$ -components of a vector respectively. The value of  $\frac{\rho}{\alpha} \mathbf{n}_{i,j}$  can then be robustly determined from Eq.(10) via *singular value decomposition* (SVD). After that, the unit vector  $\mathbf{n}_{i,j}$  is computed by normalization. As a result, we do not need to know the values of  $\rho$  and  $\alpha$  during the computation. In short, our method has no dependency on a uniform albedo. The only rule applied here is that the values

of  $\rho$  and  $\alpha$  do not change at the same surface point under the illumination of difference lighting sources.

After knowing  $\mathbf{n}_{i,j}$ , we shift the position of  $f_{i,j}$ 's vertices along the  $z$ -axis to put them on the plane  $\mathcal{P}_{i,j}$  that passes through  $\mathbf{c}_{i,j}$  and has the normal  $\mathbf{n}_{i,j}$ . A vector formed by depth components of the four projected vertices is defined as

$$\mathbf{q}(f_{i,j}) = \{p_{i,j}, p_{i+1,j}, p_{i+1,j+1}, p_{i,j+1}\}.$$

Here, the depth values are

$$p_{k,l} = \mathbf{c}_{i,j}^z - \frac{(k-i-\frac{1}{2})w\mathbf{n}_{i,j}^x + (l-j-\frac{1}{2})h\mathbf{n}_{i,j}^y}{\mathbf{n}_{i,j}^z} \quad (12)$$

with  $k \in \{i, i+1\}$  and  $l \in \{j, j+1\}$ . Note that the NLP model presented in Eq.(2) is nonlinear to the center of a facet,  $f_{i,j}$ . In our local shaping step, we simplify the computation by using the current center of  $f_{i,j}$  and leave the position of  $\mathbf{c}_{i,j}$  to be updated in the global blending step of our framework.

### C. Iteration framework for NPL-PS

The possibility allowing us to solve the NPL-PS problem by the local/global mesh deformation is based on the observation that the values of  $\{\mathbf{n}_{i,j}\}$  determined by Eq.(10) are similar to the ground truth when the initial values of  $\{\mathbf{c}_{i,j}\}$  are given in our hardware prototype. After that, when using the updated  $\{\mathbf{c}_{i,j}\}$  obtained from the global blending to generate a new set of  $\{\mathbf{n}_{i,j}\}$ , the shape is more similar to the real shape than the first update. Therefore, in our framework, these two steps are iteratively applied until the values of  $\{\mathbf{c}_{i,j}\}$  converge. More details can be found in [13], [15].

## V. EXPERIMENTAL RESULTS

The hardware of our system consists of six infrared LEDs (OSRAM SFH4232A) and one calibrated camera (Point Gray

FLFL3-U3-13S2C-CS) as shown in Fig.1. The camera is a CMOS one with resolution at  $1328 \times 1048$  pixels and has high frame-rate at about 120fps. A narrow band filter of 850nm is attached at the front of the lens to filter the visible ambient light. We install the LEDs in a circular distribution around the camera, and the chips for controlling LEDs are attached on a metal board. When capturing the images of an object to be reconstructed, our system flashes LEDs one by one to take photos by the synchronized camera. In our system, six images can be captured within 100ms. We choose infrared LEDs for lighting because that it is small enough as point source and is rarely affected by natural light. Besides, the rise and fall time of such an infrared LED is only about 0.014us, which can generate a stable intensity of lighting in a very short time.

The software part of our system is implemented by MATLAB and its performance has been tested on a variety of models in both the virtual and the real environments. The input 2D images are generated under the illumination of near point lighting. Our results are compared with that are reconstructed from the same set of 2D images but under the conventional parallel lighting assumption. All the results are generated on a PC with Intel i7 3.4GHz CPU and 8GB RAM.

#### A. Tests in virtual environment

First of all, the effectiveness of our approach is tested in a virtual environment that can generate NPL images of a 3D model with the help of OpenGL library. For each model to be tested, 27 images under the NPL illumination are generated as input to our program. To compare with the conventional PS with parallel lighting, we use the vector from a model's center to the positions of light sources as the parallel lighting directions to generate a dense normal field. After that, the *surface-from-gradients* (SfG) approach in [15] is employed to reconstruct the surface from a normal field.

A test is taken to verify the performance of our approach when the object to be reconstructed is placed at different distances from the light sources. The average errors on the normals estimated by our NPL-PS and the parallel lighting PS are measured. The testing results on the cube example are shown in Fig.7. It is found than when the model is placed far away from the light sources, both the parallel PS and our NPL-PS approaches can generate accurate results with small distortion. The reconstruction based on parallel PS becomes worse and worse when increasing the ratio between the object diameter and the object-to-light distance (i.e., reducing the object-to-light distance). However, the NPL-PS method proposed in this paper is nearly not affected. The same phenomenon is observed when the positions of light sources have been embedded with calibration errors (see the right of Fig.7).

As the ground truth is known, we can evaluate errors on both the 3D shape and the normal map obtain from the conventional PS and ours. To further verify the robustness of our approach, we randomly add errors at the level in 5% of the camera-captured region's width onto the positions of light sources. This is to simulate the calibration errors that could be embedded. Detail comparisons can be found in Figs.3-7

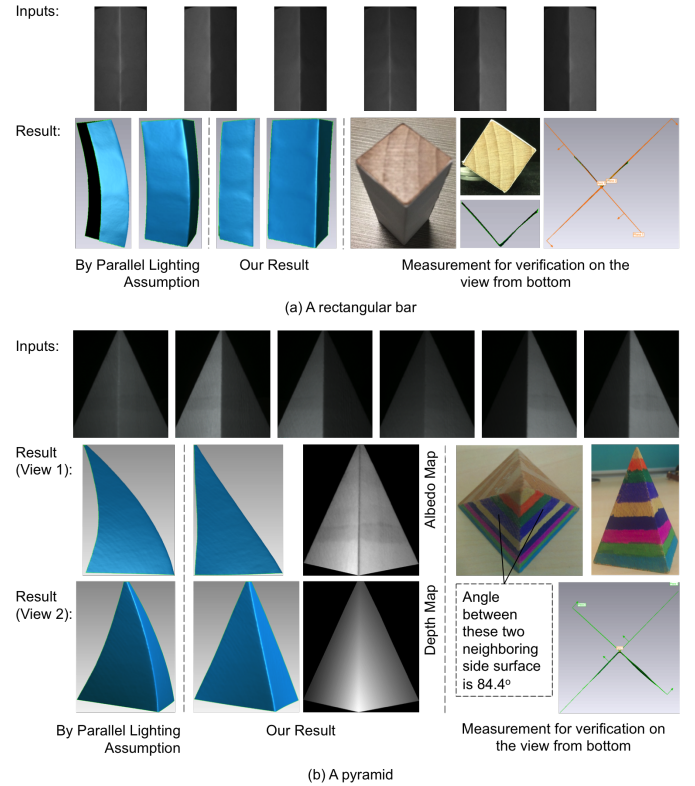


Fig. 8. Reconstruction of models with regular shape by our practical lighting system. (a) Angle between the fitting planes on the two side-surfaces is  $93.07^\circ$ , where the ground truth is  $90^\circ$ . (b) Angle between the fitting planes on the two-side surfaces of the pyramid is  $87.47^\circ$  with the ground truth  $84.4^\circ$ . Note that both the Albedo map and the depth map of the colorful pyramid model are given to demonstrate the performance of our approach on models with natural colors.

of [13]. A conclusion made by observing these comparisons is that the large distortion in PS-based reconstruction is mainly caused by the linear and nonlinear lighting assumption but not the different SfG methods. Our NPL-PS framework can generate very accurate results even under the noisy condition.

#### B. Tests on our hardware platform

The reconstruction approach is further tested in our NPL-PS hardware platform and compared to the reconstruction based on linear PS assumption (i.e., assuming to have parallel light sources). Our tests start from models with regular shape so that the quantitative error of reconstructed shape features can be easily measured. Two models, a rectangular bar and a pyramid, are used (see Fig.8). The angles between neighboring planar surfaces on the reconstructed models are measured. It can be found that very small angular errors (less than 3.5%) are presented. However, when using the parallel lighting assumption, the reconstructed surface are distorted that is caused by approximating the nonlinear relationship between lighting direction and intensity (Eq.(2)) as a linear model in Eq.(1).

More tests are taken on three statues (see Fig.9), where freeform surfaces are presented. It can be observed that the geometric details (i.e., signals in high frequency) are well preserved on both the results from conventional linear PS

TABLE I  
STATISTICS ON COMPUTING TIME<sup>†</sup>

Model	Figure	Resolution	Time
Bar	8(a)	$134 \times 266$	62 sec.
Pyramid	8(b)	$200 \times 266$	125 sec.
Statue I	9 (top)	$277 \times 516$	201 sec.
Statue II	9 (middle)	$216 \times 308$	167 sec.
Statue III	9 (bottom)	$235 \times 285$	177 sec.

<sup>†</sup>The total time of computation converging within 10 iterations is reported, where the time of pre-factorization has been included.

and our results. However, structural shape distortions (in low frequency) are presented on the results obtained by using parallel lighting assumption. When comparing the profiles of reconstructed models to the real objects shown in the photographs, a ‘global’ spherical distortion can be found on the results from conventional PS. This is mainly caused by the difference between the assumed parallel and the spherical scattered lighting directions in practice. As illustrated in Fig.2(b) and (c), when the dot product between lighting and normal are given according to the light intensity  $I_i(\mathbf{x})$ , assuming parallel lighting in a NPL scenario leads to a spherically distorted distribution of surface normals. Specifically, the actual lighting directions scatter from one point (the light source) in NPL. The resultant normal vectors will be inversely scattered if the assumption of parallel lighting is applied (see Fig.2(c)). This will then result in a spherical distortion on the reconstructed surface. The comparison results also provide a confidence to justify the correctness of our NPL-PS formulation in Eq.(2). Lastly, natural objects – a peach is tested and shown in Fig.10. In summary, our system can reconstruct less distorted 3D geometry under the near point light illumination.

### C. Computing time

The local/global deformation based computation can solve the nonlinear NPL-PS problem in a very efficient way. Statistics of applying our approach on input images with rectangular domain in different resolutions are listed in Table I. The statistics are generated on our primary implementation in MATLAB. We plan to implement our approach by C++ to further improve the efficiency of computation in the near future.

## VI. CONCLUSION

In this paper, we present a practical lighting system with near point lighting for dense reconstruction by using photometric stereo. To solve the problem of surface reconstruction under a near point lighting condition which is in fact a nonlinear problem, a novel computational framework is developed. Specifically, the nonlinear PS problem is formulated in a pure geometry way and then solved through iterative local/global mesh deformations. The surface normals and depths can be simultaneously estimated in our approach. The positions of point light sources are obtained via a calibration process. The effectiveness of our method has been demonstrated using

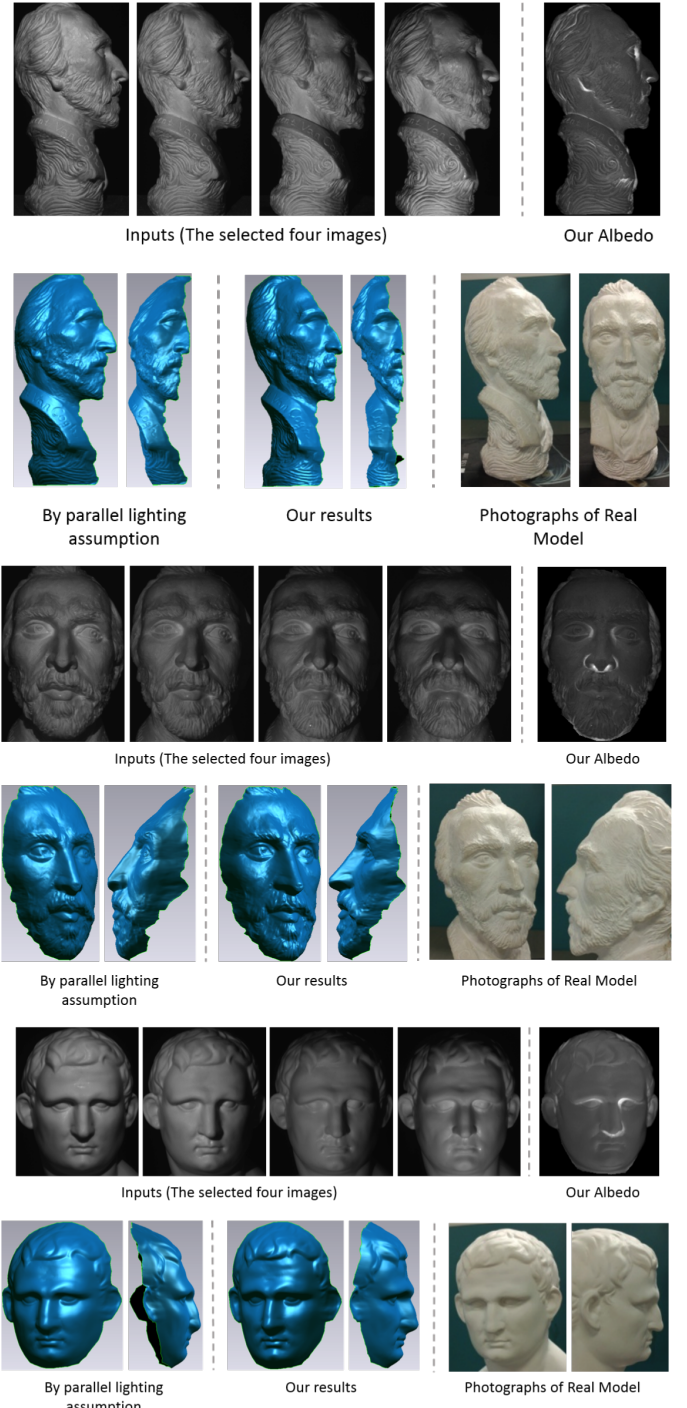


Fig. 9. Reconstruction of statue models with freeform surface. Our method does not rely on the assumption of uniform albedo – see the distribution shown in the upper-right corner of each result.

synthetic images with calibration errors considered. A hardware setup for NPL-PS has been constructed to further verify the performance of our technique presented in this paper. The distinct advantage of this new technique is its ability to efficiently generate dense 3D depth maps in high accuracy. To the best of our knowledge, this has not been realized by any prior method. On the other aspect, the current formulation is based on the ideal Lambertian reflection. It will be interesting

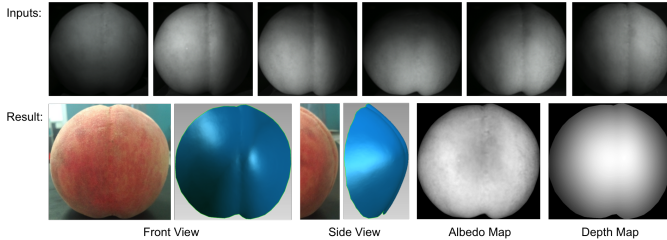


Fig. 10. Reconstruction of a peach model with freeform surface. Our method does not rely on the assumption of uniform albedo – see the distribution shown in the Albedo map.

if a more real reflection model can be used in the future to reconstruct more natural objects.

#### ACKNOWLEDGMENT

This research is partially supported by National Natural Science Foundation of China (Grant No.: 61375041) and Shenzhen Science Plan (Grant No.: JCY20140509174140685 and JCYJ20150401150223645). We acknowledge Zhao SONG for his efforts on the hardware and experiments during the revision of this paper.

#### REFERENCES

- [1] S. Barsky and M. Petrou, “The 4-source photometric stereo technique for three-dimensional surfaces in the presence of highlights and shadows,” *IEEE Transactions on Pattern Analysis and Machine Intelligence*, vol. 25, no. 10, pp. 1239–1252, 2003.
- [2] A. Wetzler, R. Kimmel, A. M. Bruckstein, and R. Mecca, “Close-range photometric stereo with point light sources,” in *2014 2nd International Conference on 3D Vision (3DV)*, 2014, pp. 115–122.
- [3] W. Xie, Z. Song, and R. Chung, “Real-time three-dimensional fingerprint acquisition via a new photometric stereo means,” *Optical Engineering*, vol. 52, no. 10, 2013.
- [4] L. Xie, Z. Song, and X. Huang, “A novel method for the calibration of an led-based photometric stereo system,” in *Information and Automation (ICIA), 2013 IEEE International Conference on*, Aug 2013, pp. 780–783.
- [5] Y. Iwahori, H. Sugie, and N. Ishii, “Reconstructing shape from shading images under point light source illumination,” in *Pattern Recognition, 1990. Proceedings., 10th International Conference on*, 1990, pp. 83–87.
- [6] J. J. Clark, “Active photometric stereo,” in *Computer Vision and Pattern Recognition, 1992. Proceedings CVPR '92., 1992 IEEE Computer Society Conference on*, Jun 1992, pp. 29–34.
- [7] Z. Zhou and P. Tan, “Ring-light photometric stereo,” in *ECCV 2010: 11th European Conference on Computer Vision*, 2010, pp. 265–279.
- [8] J. J. Clark, “Photometric stereo using {LCD} displays,” *Image and Vision Computing*, vol. 28, no. 4, pp. 704–714, 2010.
- [9] J. Wang, Y. Matsushita, B. Shi, and A. C. Sankaranarayanan, “Photometric stereo with small angular variations,” in *IEEE Intl. Conf. Computer Vision (ICCV)*, 2015.
- [10] M. K. Johnson, F. Cole, A. Raj, and E. H. Adelson, “Microgeometry capture using an elastomeric sensor,” *ACM Transactions on Graphics (Proc. ACM SIGGRAPH)*, vol. 30, no. 4, pp. 46:1–46:8, 2011.
- [11] T. Higo, Y. Matsushita, N. Joshi, and K. Ikeuchi, “A hand-held photometric stereo camera for 3-d modeling,” in *IEEE International Conference on Computer Vision*, 2009, pp. 1234–1241.
- [12] M. Liao, L. Wang, R. Yang, and M. Gong, “Light fall-off stereo,” in *2007 IEEE Conference on Computer Vision and Pattern Recognition*, 2007, pp. 1–8.
- [13] W. Xie, C. Dai, and C. C. L. Wang, “Photometric stereo with near point lighting: A solution by mesh deformation,” in *Computer Vision and Pattern Recognition (CVPR), 2015 IEEE Conference on*, 2015, pp. 4585–4593.
- [14] S. Bouaziz, M. Deuss, Y. Schwartzburg, T. Weise, and M. Pauly, “Shape-up: Shaping discrete geometry with projections,” *Comptuer Graphics Forum*, vol. 31, no. 5, pp. 1657–1667, 2012.
- [15] W. Xie, Y. Zhang, C. Wang, and R.-K. Chung, “Surface-from-Gradients: An approach based on discrete geometry processing,” in *IEEE Conference on Computer Vision and Pattern Recognition (CVPR)*, 2014, pp. 2203–2210.
- [16] T. Higo, Y. Matsushita, and K. Ikeuchi, “Consensus photometric stereo,” in *IEEE Conference on Computer Vision and Pattern Recognition*, 2010.
- [17] Z. Zhang, “A flexible new technique for camera calibration,” *IEEE Trans. Pattern Anal. Mach. Intell.*, vol. 22, no. 11, pp. 1330–1334, Nov. 2000.
- [18] W. Zhou and C. Kambhamettu, “Estimation of illuminant direction and intensity of multiple light sources,” in *Proceedings of the 7th European Conference on Computer Vision-Part IV*, ser. ECCV '02, 2002, pp. 206–220.
- [19] D. Nehab, S. Rusinkiewicz, J. Davis, and R. Ramamoorthi, “Efficiently combining positions and normals for precise 3d geometry,” *ACM Trans. Graph.*, vol. 24, no. 3, pp. 536–543, 2005.
- [20] D. Goldman, B. Curless, A. Hertzmann, and S. Seitz, “Shape and spatially-varying brdfs from photometric stereo,” *IEEE Transactions on Pattern Analysis and Machine Intelligence*, vol. 32, no. 6, pp. 1060–1071, 2010.
- [21] L. Wu, A. Ganesh, B. Shi, Y. Matsushita, Y. Wang, and Y. Ma, “Robust photometric stereo via low-rank matrix completion and recovery,” in *Proceedings of 2011 ACCV Conference*, 2011, pp. 703–717.
- [22] F. Lu, Y. Matsushita, I. Sato, T. Okabe, and Y. Sato, “Uncalibrated photometric stereo for unknown isotropic reflectances,” in *Proceedings of the 2013 IEEE Conference on Computer Vision and Pattern Recognition*, 2013, pp. 1490–1497.
- [23] Z. Song, R. Chung, and X. Zhang, “An accurate and robust strip-edge based structured light means for shiny surface micro-measurement in 3D,” *IEEE Transactions on Industrial Electronics*, vol. 60, no. 3, pp. 1023–1032, 2013.
- [24] Y. Zhang, G. M. Gibson, R. Hay, R. W. Bowman, M. J. Padgett, and M. P. Edgar, “A fast 3D reconstruction system with a low-cost camera accessory,” *Scientific Reports*, vol. 5, 2015.
- [25] H. Du and Z. Wang, “Three-dimensional shape measurement with an arbitrarily arranged fringe projection profilometry system,” *Optics Letters*, vol. 32, no. 16, pp. 2438–2440, 2007.
- [26] M. Demeyere, D. Rurimunzu, and C. Eugene, “Diameter measurement of spherical objects by laser triangulation in an ambulatory context,” *Instrumentation and Measurement, IEEE Transactions on*, vol. 56, no. 3, pp. 867–872, June 2007.
- [27] R. Lange and P. Seitz, “Seeing distances - a fast timeofflight 3D camera,” *Sensor Review*, vol. 20, no. 3, pp. 212–217, 2000.